

Novel two-dimensional materials from high-throughput computational exfoliation of experimentally known compounds

Nicolas Mounet,¹ Marco Gibertini,¹ Philippe Schwaller,¹ Andrius Merkys,¹
Ivano E. Castelli,¹ Andrea Cepellotti,¹ Giovanni Pizzi,¹ and Nicola Marzari¹

¹*Theory and Simulation of Materials (THEOS) and National Centre for Computational Design and Discovery of Novel Materials (MARVEL), École Polytechnique Fédérale de Lausanne, 1015, Switzerland*

We search for novel two-dimensional materials that can be easily exfoliated from their parent compounds. Starting from 108423 unique, experimentally known three-dimensional compounds we identify a subset of 5619 that appear layered according to robust geometric and bonding criteria. High-throughput calculations using van-der-Waals density-functional theory, validated against experimental structural data and calculated random-phase-approximation binding energies, allow to identify 1844 compounds that are either easily or potentially exfoliable, including all that are commonly exfoliated experimentally. In particular, the subset of 1053 easily exfoliable cases—layered materials held together mostly by dispersion interactions and with binding energies in the range of few tens of $\text{meV} \cdot \text{\AA}^{-2}$ —contains several hundreds of entries with few atoms per primitive cell (273 with less than 6 atoms, 606 with less than 12), revealing a wealth of new structural prototypes, simple ternary compounds, and a large portfolio to search for optimal electronic, optical, magnetic, topological, or chemical properties.

Two-dimensional (2D) materials provide novel opportunities to venture into largely unexplored regions of the materials properties space. On one hand, their ultimate thinness makes them extremely promising for applications in electronics (e.g., for field-effect transistors, where a reduced device size is beneficial to improve performance and reduce short-channel effects between contacts).^{1–4} On the other hand, the physical properties of monolayers often change dramatically from those of parent 3D materials, providing a new degree of freedom⁵ in the applications (from thermoelectrics to spintronics) while also unveiling novel physics (e.g., valley Hall effect and composite excitations such as trions). Moreover, van-der-Waals (vdW) heterostructures⁶ have recently emerged as an additional avenue to engineer novel properties by stacking 2D materials in a specifically designed fashion.

Still, to date only a few dozens of 2D materials have been experimentally synthesised or exfoliated. Progress in this area would be strongly accelerated by the availability of a broader portfolio of potential realistic 2D materials. To illustrate this point, we can compare the current situation for known 3D crystals, for which the knowledge accumulated in the past century (both the crystal structure and the measured physical properties) has been collected in databases such as the Pauling file⁷, the Inorganic Crystal Structure Database⁸ (ICSD) or the Crystallographic Open Database⁹ (COD) (the latter two, combined, contain to date over half a million entries). In comparison, 2D materials databases are still scarce and limited in size: a first systematic scan of the ICSD database providing 92 two-dimensional compounds has been provided in Ref. 10, followed by 103 compounds selected among specific classes of materials¹¹; finally a recent study focused on transition-metal dichalcogenides and oxides, identifying 51 of them as stable¹².

In order to fill this knowledge gap, high-throughput computational methods represent a promising tool¹³ that

has proven to be extremely effective in screening materials without the need to synthesise them first^{14–18}. For instance, these techniques have been successfully employed in the search for novel materials for Li-air and Li-ion batteries^{19,20}, for hydrogen storage²¹, electrocatalysis^{22,23}, or to accelerate the discovery of novel light-absorbing²⁴ and light-harvesting^{25,26} materials.

In this work, we start from geometric and bonding criteria to identify layered materials among the compounds contained in the ICSD and COD databases, independently of the layers' shape, crystallographic orientation or embedding. We then use first-principles vdW density-functional theory (DFT) simulations to validate these results. In particular, we compute the binding energy of all prospective layered structures and identify those that are held together by weak interactions and ready for mechanical²⁷ or liquid-phase²⁸ exfoliation²⁹. This results into a database of 1844 exfoliable 2D materials.

The reproducibility of the complete study is ensured by the AiiDA³⁰ materials' informatics infrastructure, which keeps track of the provenance of each calculation and result.

I. RESULTS AND DISCUSSION

Starting set of three-dimensional structures

The computational exfoliation protocol starts from a comprehensive initial set of bulk 3D crystal structures. These are extracted from databases of experimental compounds, and for this study we focused on the ICSD⁸ and COD⁹, containing respectively 177343 (ICSD 2015.1) and 351589 entries (COD Rev. #171462). Entries containing at most 6 different species are retrieved in the form of CIF files³¹ using routines distributed within the AiiDA

platform³⁰, and passed through successive cod-tools filters³² to correct typical syntax errors that prevent the successful reconstruction of the intended crystal structures (see Methods for more details). Entries with partial occupancies in the unit cell are then filtered out, together with CIF files that do not provide the explicit position of one or several atoms, cannot be parsed, or are obviously wrong. Purely theoretical structures are also discarded.

The CIF files are then converted into AiiDA structures using the pymatgen³³ parser. The spglib software³⁴ is subsequently used to find the primitive cells and to refine the atomic positions, in order to avoid unwanted loss of crystal symmetries due to round-off errors (see Methods for more details). Finally, duplicate structures (found using the pymatgen structure matcher³⁵ - see Methods) are removed from our initial set of 3D structures. The removal of duplicates is done first independently on each of the ICSD and COD sets. Then, every structure of the ICSD set for which there exists a similar structure inside the COD is also removed. This procedure provides a starting set of 108423 unique 3D crystal structures, to be further investigated.

2D screening algorithm

The 3D structures classified as unique can then be analysed to find promising candidates for exfoliation into one or several 2D materials. The first step consists in identifying composite structures, i.e., structures that can be decomposed into disconnected units held together by weak interactions. A pioneering attempt in this direction has been put forward by Lebègue and coauthors¹⁰ even if limited to high-symmetry compounds with layers perpendicular to the [001] crystal axis. A versatile algorithm is however needed in order to cope with the following general and realistic situations:

- layered structures belonging to any crystal system (obvious exceptions are the cubic systems³⁶);
- orientation of the stacking direction not along the [001] axis (see, e.g., Fig. 1b);
- layers apparently outside the 3D primitive unit cell, requiring the use of sufficiently large supercells to check for connectivity (see, e.g., Fig. 1c);
- layers that are interpenetrating, i.e. with overlapping projections along the stacking direction (see, e.g., Fig. 1d);
- composite structures that include units with different dimensionalities (see, e.g., Fig. 1e);
- different chemical environment affecting the typical bond distance between atoms, requiring some tolerance in the screening parameters.

Here we provide a protocol that is able to deal with all the scenarios above and identify layers that can then be

fed into first-principles calculations. The goal is to automatically find chemically-bonded manifolds in a given structure, and among them select those that are periodic in two independent directions.

The fundamental steps are reported schematically in Fig. 1a. First, from the bulk primitive cell of the 3D candidate a $3 \times 3 \times 3$ supercell is created. All interatomic distances are evaluated and chemical bonds are identified as those for which

$$d_{i,j} < r_i^{\text{vdW}} + r_j^{\text{vdW}} - \Delta, \quad (1)$$

where $d_{i,j}$ is the distance between two atoms i and j , r_i^{vdW} is the van-der-Waals radius of atom i as obtained from Alvarez (Ref. 37), and Δ is a parameter that we specify below. The criterion in (1) is based on the statistical analysis of the distribution of over five million interatomic distances, according to which Alvarez pointed out that covalent bonds are likely to form only when the distance between atoms is shorter than the sum of the vdW radii by more than a quantity Δ (on average equal to 1.3 Å). Thus, if the interatomic distance is smaller than $r_i^{\text{vdW}} + r_j^{\text{vdW}} - \Delta$ as required by Eq. (1), then the two atoms should be chemically connected. On the contrary, if the interatomic distance is larger than this, then any kind of strong chemical bonding should be absent and only vdW interactions remain (some special case involving hydrogen or metallic bonding are still possible and discussed in Ref. 37, but we will not consider them here). In our analysis we have considered five equally spaced values for Δ between 1.1 Å and 1.5 Å to account for possible uncertainties in the values of the vdW radii and of Δ itself. We believe that a criterion based on vdW radii could be more robust and versatile than one based on covalent radii, as it allows to take into account the unavoidable bond-length fluctuations associated with different chemical environments.

As soon as all bonds are identified, chemically connected groups are constructed. $3 \times 3 \times 3$ supercells are needed to correctly describe cases when a group of bonded atoms spans a total of three unit cells in a given direction, as illustrated in Fig. 1c. In principle, even such supercells might not be large enough in some rare cases, although the algorithm could then be applied to even larger supercells.

The dimensionality of each connected group is obtained from the rank of the set of vectors linking an atom to all of its chemically connected periodic images (periodic according to the 3D lattice vectors). This approach is general and does not assume any specific orientation of the 2D plane with respect to the crystal or Cartesian axes. Moreover, it also identifies and returns other low-dimensional units, such as 1D chains or 0D clusters.

Applying the full protocol to all 108423 unique 3D structures, we found 5619 layered materials that can be considered as potential parents of 2D monolayers.

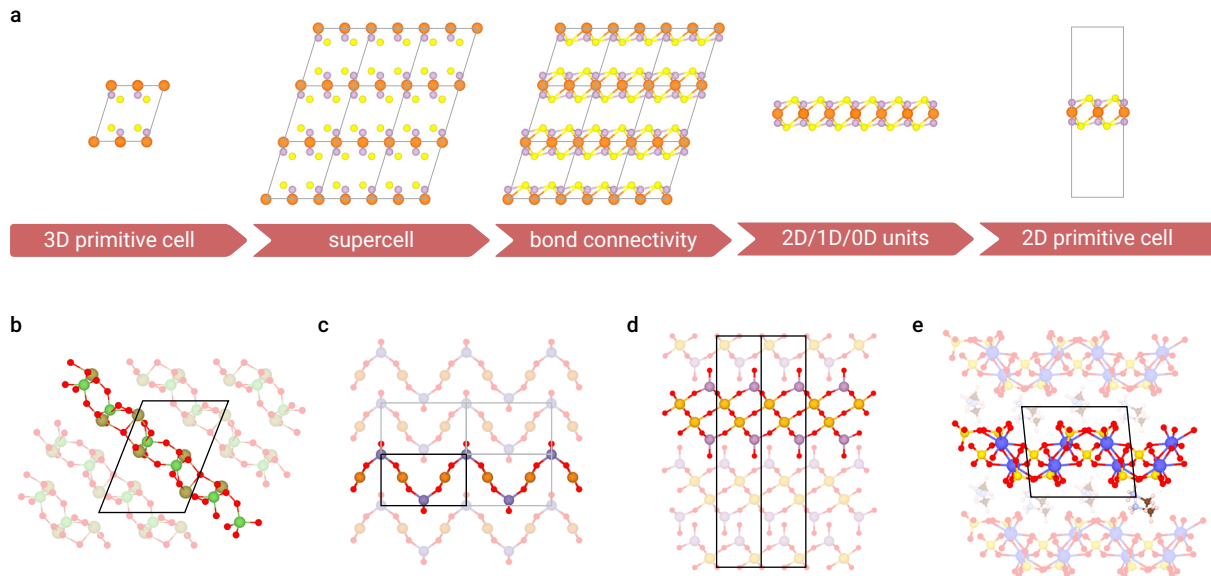


FIG. 1. **a** Schematic representation of the fundamental steps needed to find low-dimensional units of a parent 3D crystal (here MgPS_3). **b-e** Examples illustrating non-trivial layered structures that can be identified in: **b** Triclinic or monoclinic structures that are not layered along the $[001]$ crystallographic direction ($\text{As}_2\text{Te}_3\text{O}_{11}$, from ICSD #425299). **c** Layered compounds whose constitutive layers extend over multiple unit cells and that thus require the use of supercells to be identified (CuGeO_3 , from COD #1520902). **d** Layers that have partial overlap of the atomic projections along the stacking direction, with no manifest vacuum separation between them ($\text{Mo}_2\text{Ta}_2\text{O}_{11}$, from ICSD #247163). **e** Composite structures that contain units with different dimensionality ($(\text{CH}_6\text{N})_2(\text{UO}_2)_2(\text{SO}_4)_3$, from ICSD #192165, where 2D layers of uranyl sulphate are intercalated with 0D methylammonium molecules).

Structural relaxation and comparison with experiments

The geometrical screening described in the previous section provides an exhaustive list of potential candidates for exfoliation. Although an important first step, this geometrical characterization is not sufficient and has to be complemented with accurate calculations in order to identify materials that do actually exhibit weak interlayer bonding and are easily exfoliable. Here we use vdW DFT simulations to proceed with such a refinement (computational details can be found in the Methods).

The first step is the optimization of the 3D geometry (cell vectors and atomic positions) of the layered structures found. This procedure is completely automated within AiiDA. Preference is given to the simplest structures, both for their higher relevance and for computational efficiency. As a result, at least all unary compounds containing less than 100 atoms in the unit cell, all binaries and ternaries with less than 40 atoms, and all other quaternary, quinary, and senary compounds with less than 32 atoms are considered; in total, 3210 layered compounds have been studied with first-principles calculations. These structures are relaxed using two different non-local vdW-compliant functionals: the vdW-DF2 functional³⁸ with C09 exchange^{39,40} (DF2-C09) and the revised Vydrov-Van Voorhis⁴¹⁻⁴³ (rVV10) functional.

To assess the accuracy in predicting the equilibrium

structure for the functionals adopted, we compare the experimental interlayer distance (defined as the distance between the geometrical centres of neighbouring layers) of a subset of layered materials against computational predictions. The results are shown in Fig. 2, complemented also by the semi-local Perdew-Burke-Ernzerhof (PBE)⁴⁴ and the revPBE⁴⁵ functionals. Since revPBE and PBE are not designed to predict vdW interactions, discrepancies with experiments are larger, as seen in Fig. 2a-b. On the contrary, the two vdW-compliant functionals provide interlayer distances closer to experimental values and with a much smaller dispersion around the average (see Fig. 2c-d), and are able to correctly predict the structural properties of non-closely-packed materials (including vdW-bonded structures). This can be quantified by looking at the mean absolute percentage errors (1.5% for both vdW-DF2-C09 and rVV10, against 10% and 4% for revPBE and PBE, respectively).

Moreover, the low mean relative errors of vdW-DF2-C09 and rVV10 predictions (-1% and -0.3% , respectively) show that these functionals have no bias in determining the equilibrium interlayer distance of layered structures, while revPBE and PBE have a tendency to underbind that is emphasised at smaller packing ratios.

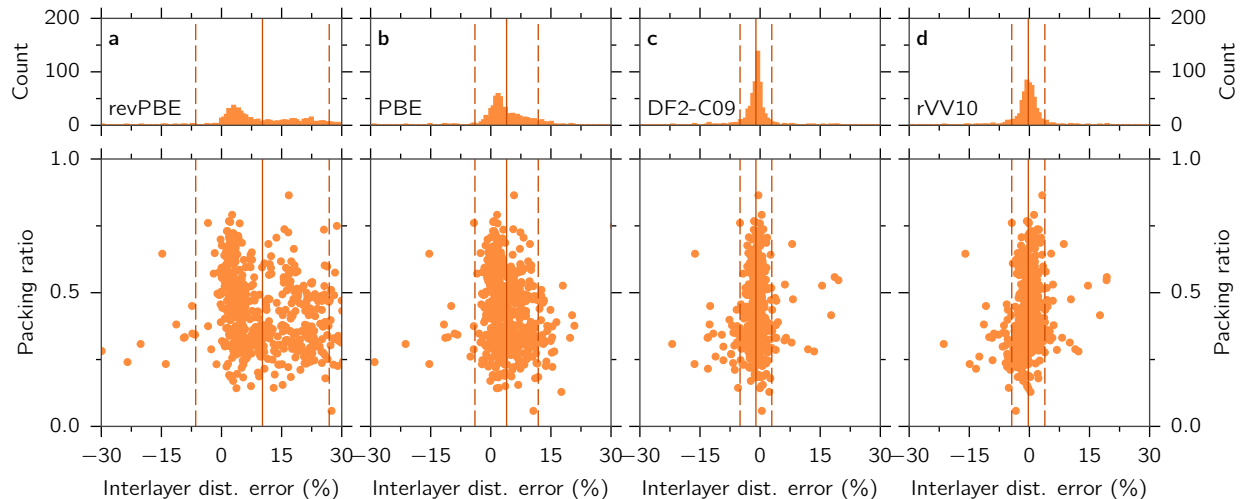


FIG. 2. Top panels: distribution of the relative error in the interlayer distance calculated with DFT with respect to the value for the corresponding experimental structure, for 573 layered materials identified by the geometrical screening for which the structure has been explicitly marked as experimental in the parent database, and for which a relaxation has been performed with all four exchange-correlation functionals. The four functionals considered are: **a** the revPBE functional, **b** the PBE functional, **c** the DF2 non-local vdW functional with C09 exchange, **d** the revised VV10 non-local vdW functional. Vertical solid lines are located at the distribution average, while dashed lines are located two standard deviations away from the average (we removed outliers when calculating the position of these lines, outliers being defined as data points sitting in bins with less than three counts, with a bin width of 0.6%). Lower panels: Scatter plot of the packing ratio versus the interlayer distance error.

Binding energies and final selection of exfoliable materials

To go further in the selection of 2D materials, we need to determine if the interlayer interactions are weak enough for the parent compound to be a good candidate for exfoliation. After the structural optimization described previously, one can proceed with exfoliation, i.e., separation into several substructures as described earlier. If the exfoliation produces one or several two-dimensional structures, the ground-state energy of each isolated unit is computed. Note that, due to the change in atom positions and thus of bond lengths, DFT optimization leads in certain cases to a non-exfoliable structure, even if the initial 3D parent directly extracted from the ICSD or COD was classified as layered.

The ground-state energy difference between the 3D bulk and all of its substructures (of any dimensionality, including also 1D chains or 0D clusters) gives the binding energy E_b , closely related to the exfoliation energy, i.e., the energy needed to exfoliate one layer out of a multilayer system⁴⁶. Here E_b is chosen to be positive when the bulk is more stable than its individual low-dimensional constituents. We show in Fig. 3a the binding energies per layer and per unit surface obtained for well-known layered materials including graphite, hexagonal boron nitride and several transition-metal dichalcogenides. The values obtained with the two vdW functionals are in very good agreement with accurate reference calculations performed in Ref. 46 using the random phase approxima-

tion (RPA). For all these compounds (except PdTe₂) the binding energies range between 20 and 40 meV · Å⁻². We then show in Fig. 3b the distribution of the binding energies for the 2662 systems studied in this work. For both vdW functionals, a majority of compounds (resp. 74% for DF2-C09 and 71% for rVV10) exhibit a binding energy smaller than 100 meV · Å⁻², giving rise to a first very high peak in the distribution (notice the logarithmic scale). A second broader peak appears between 200 and 400 meV · Å⁻² and is associated with structures containing also lower dimensionality units (i.e., 0D or 1D) in addition to the 2D layer(s). The larger binding energy is to be expected for structures with mixed dimensionality (typically 0D and 2D) where charge transfer between intercalated units and 2D layers can take place giving rise to ionic bonds, as in the case of NaSb₂As₂⁴⁷. This means that these additional 0D or 1D substructures could have been erroneously separated from the 2D layers in the geometrical screening.

The binding energies distribution is quite continuous. As a result, a criterion to select layered materials solely based on the binding energy is difficult to define without a level of arbitrariness. To lift this ambiguity, we correlate the binding energy with the relative discrepancy in interlayer distance obtained in vdW and non-vdW DFT calculations, using for the non-vdW simulations the revPBE functional⁴⁵ that, contrary to standard PBE, does not seem to display bonding interaction in the exchange energy⁴⁸. We plot in Fig. 3c this binding en-

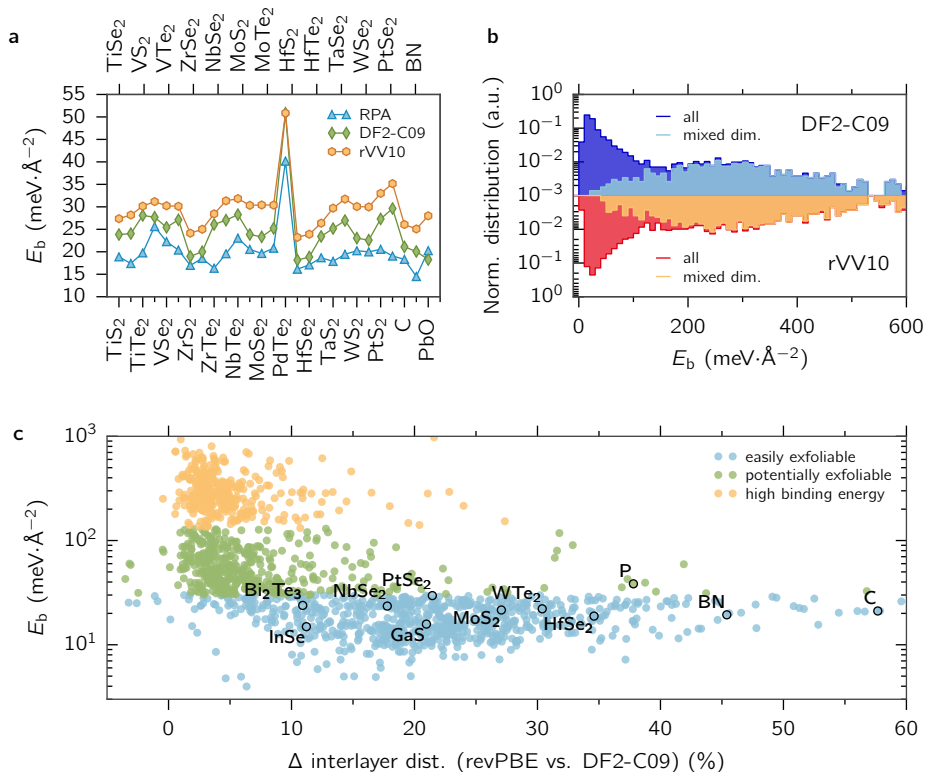


FIG. 3. Binding energies of the bulk 3D compounds identified as geometrically layered: **a** Binding energy for a selection of layered materials identified in Ref. 46, comparing results from RPA (Ref. 46) and from the DF2-C09 and rVV10 functionals (this work). **b** Normalised distribution of all binding energies computed in this work. **c** Binding energy vs relative discrepancy in interlayer distance between the structure relaxed using the revPBE and the DF2-C09 functional. Materials classified as easily exfoliable, potentially exfoliable, or with high binding energy are reported in different colours. Well-known 2D materials are highlighted in the plot.

ergy against the interlayer-distance difference for 1535 compounds that have been studied with the revPBE and DF2-C09 functionals. We observe that most compounds with low binding energy exhibit a large relative discrepancy in interlayer distance calculated with the two functionals, which is expected since the interlayer interaction is very sensitive to vdW forces. This allows us to identify which layered compounds are characterised by vdW interactions between layers. We set the threshold for these (shown in blue in Fig. 3c) at $30 \text{ meV} \cdot \text{\AA}^{-2}$ for binding energies computed with the DF2-C09 functional, and $35 \text{ meV} \cdot \text{\AA}^{-2}$ for those computed using rVV10. We classify two-dimensional systems exfoliated from compounds belonging to this group as “easily exfoliable” (EE). As shown in Fig. 3c, this choice recovers 2D materials commonly exfoliated in experiments⁴⁹, validating the approach.

At the top left of Fig. 3c, a number of compounds exhibit high binding energies and a similar interlayer distance when comparing the revPBE and vdW functionals; many also contain substructures of mixed dimensionali-

ties, as discussed before. This group can be clearly separated from the rest, and is shown in yellow in Fig. 3c, the boundary being set at $130 \text{ meV} \cdot \text{\AA}^{-2}$ for both functionals. Above this value, compounds are not considered exfoliable and they are discarded from the database.

Between these two regions, compounds with intermediate binding energies (in green in Fig. 3c) exhibit a relatively weak, possibly non-vdW, bonding. As an example, the compound PdTe₂ discussed above belongs to this region, and is metallic out-of-plane. We classify two-dimensional structures exfoliated from parents belonging to this group as “potentially exfoliable” (PE).

Finally, materials for which the binding energy has been computed with both vdW functionals are classified according to the most optimistic prediction.

The 2D database

Using these criteria, and after removal of duplicates (see Methods), we obtain 1053 easily exfoliable and 791

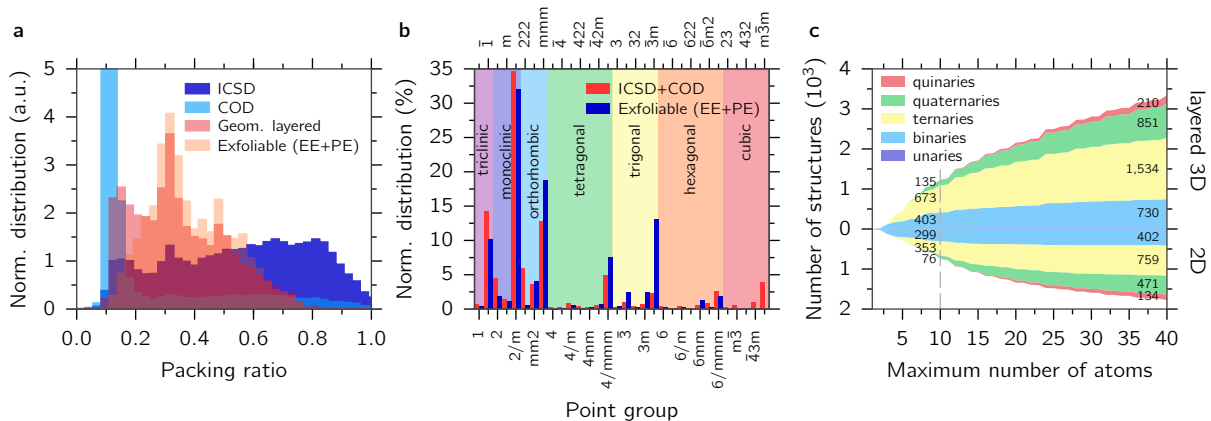


FIG. 4. Statistics on the 2D and 3D databases: **a** Packing ratios for the 3D structures considered, layered compounds and exfoliable materials. **b** Distribution of point groups. **c** Number of structures as a function of the number of atoms in the primitive cell (top: layered 3D structures; bottom: 2D structures in the EE and PE groups combined). The number of structures with at least two different species is explicitly reported for a maximum number of atoms equal to 10 and 40. The number of unary structures with less than 10 (40) atoms is 13 (15) for 3D layered compounds and 15 (15) for 2D EE+PE materials.

potentially exfoliable compounds, for a total of 1844 candidates (Table I summarises all different steps). In Fig. 4 we plot some statistics for this portfolio of promising materials, as well as for their 3D parents: We show the distribution of packing ratios in the ICSD and COD structures, in the group of 3D layered compounds, and in the EE and PE ones, using covalent radii⁵⁰ to compute the atomic volume. While the initial databases contain many closely packed structures with packing ratios of 0.7 or more, the layered structures are peaked around low packing ratios (0.3) but with a spread extending up to 0.8, even in the final set of exfoliable compounds. These considerations highlight how the packing ratio alone is not necessarily a good criterion to filter 2D structures. (Note that the peak of COD at a packing ratio of 0.15 – which goes beyond the upper limit of the graph – is due to the fact that COD is populated with a large number of molecular crystals, microporous networks, metal-organic frameworks, and zeolites.)

Then, in Fig. 4b we show the distribution of point groups, arranged by crystal system, in all 3D structures, compared to that of the exfoliable 3D compounds. Most point groups are represented similarly in both sets, with the notable exception of all cubic point groups that are obviously absent from the set of layered compounds. Moreover, the 222 point group is much rarer in the layered compounds than in the ICSD and COD databases, while the 3m, $\bar{3}$, $\bar{3}m$ and 6mm point groups are conversely more present among 3D exfoliable compounds. It is interesting to note that while most of the 2D materials studied in the last ten years belong to the hexagonal crystal system, these structures represent only a minority of the full database of exfoliable materials.

Finally, in Fig. 4c we show how the layered and 2D compounds are distributed in terms of the number of

species and number of atoms in the unit cell. As apparent from the graph, there are hundreds of 2D structures with few atoms in the unit cell (273 with less than 6 atoms, 606 with less than 12 atoms), that can be used as a starting set for screening 2D materials with desired properties. We find 18 2D structures containing a single species, including all known exfoliable 2D unaries such as graphene and phosphorene. Novel unaries belong to the class of PE materials and mostly arise from intercalation layers in the parent 3D structures; they are typically not mechanically stable. Interestingly, ternary 2D materials, which have been so far largely unexplored, represent a significant fraction of structures with less than 10 atoms in the unit cell, demonstrating that it may be worth inspecting these more versatile compounds beyond the current realm of unary/binary 2D materials.

In order to provide a more precise overview, we further classify the 2D materials of the EE group into different prototypes, according to their spacegroups and their structural similarity, when the species are all considered undistinguishable and only the stoichiometry matters (for this we use the pymatgen structure matcher – see Methods for more details). 566 prototypes are found, among which the ten most common ones represent a total of 219 structures and are shown in Fig. 5. The most common structural prototype is that of CdI₂, which groups together 67 similar structures, including many transition-metal dichalcogenides and dihalides. Contrary to the general distribution of point groups in Fig. 4b, most of these prototypes have high-order rotation axes, with the only exception being the rectangular FeOCl. Although some of these structures have already been suggested as exfoliable¹⁰, the abundance of some relatively complex prototypes involving more than two species is new and compelling. Moreover, we emphasise that the NdTe₃ pro-

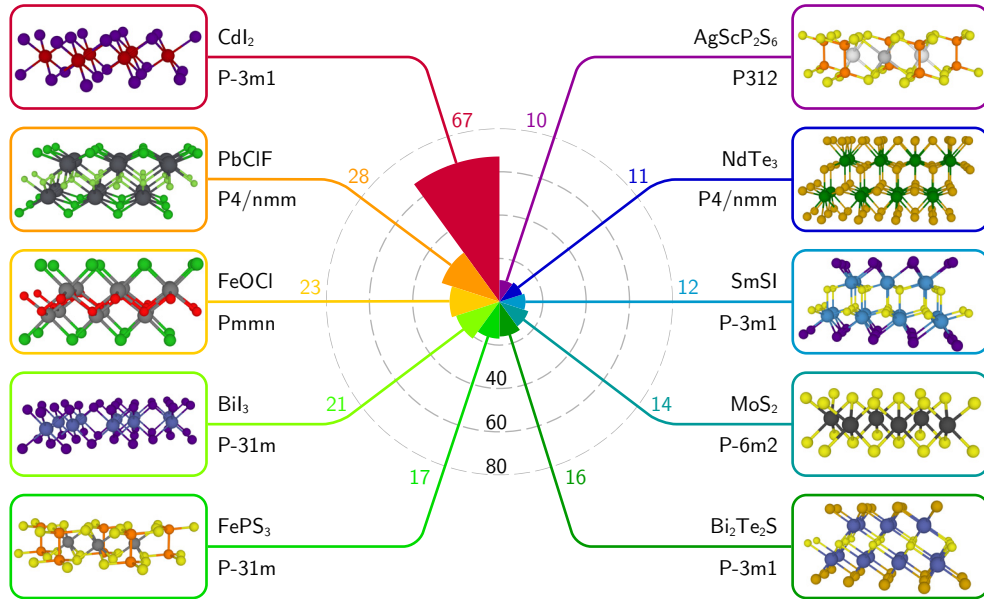


FIG. 5. Polar histogram with the number of structures belonging to the ten most common 2D structural prototypes in the set of easily exfoliable 2D materials. A graphical representation of each prototype is reported, together with the structure-type formula and the spacegroup of the 2D systems.

	Unique to ICSD	Unique to COD	Common to both	Total sum
Experimental data				
CIF inputs	99212	87070		186282
Unique 3D structures	34548	60354	13521	108423
Layered 3D structures	3257	1180	1182	5619
DFT calculations (PBE, revPBE, DF2-C09 and rVV10)				
Layered 3D, relaxed	2165	175	870	3210
Binding energies	1795	126	741	2662
2D easily exfoliable (EE)	672	81	300	1053
2D pot. exfoliable (PE)	521	36	234	791
Total	1193	117	534	1844

TABLE I. Number of CIF files imported from the two databases (ICSD or COD, uniqueness not tested), number of unique 3D structures in each imported set or common to both, and number of layered 3D structures identified using the geometrical criteria discussed in the text. Number of DFT calculations (performed with at least one of the 4 different exchange-correlation functionals) for the atomic/cell relaxations of these geometrically layered structures, for the binding energies of the constituent 2D structures, and number of 2D structures that satisfy the additional criteria for easy or potential exfoliation (see text).

prototype has not been reported before and it is common to many rare-earth tritellurides.

II. CONCLUSION

We identified an extensive database of exfoliable materials by systematic analysis and screening of structures from both the ICSD and the COD structural databases. We developed a geometrical algorithm to select potentially layered materials that is general enough to recognise substructures independently of their crystallographic orientation, dimensionality and environment. The list of 2D materials obtained by geometrical considerations is then tested against accurate, validated vdW-DFT computations of the binding energies for all layers identified. Compounds with sufficiently small binding energies and where dispersion relations affect interlayer distances are deemed exfoliable. The materials identified are in particular classified into groups of easily (1053) or potentially (791) exfoliable compounds, showing how only a very small fraction of possible 2D materials has been considered up to now. In particular, many opportunities might arise from materials with reduced symmetry or involving more than two atomic species but still with relatively simple structures. From the identification of the most common structural prototypes, we suggest that materials displaying promising properties like ferromagnetic insulators or tunable superconductors actually belong to larger families of structures that potentially contain novel materials with even more compelling characteristics. All results can be fully reproduced thanks to the deployment of the AiiDA infrastructure that tracks the provenance of each data entry. To date, this is the largest available database of 2D compounds.

III. METHODS

A. Reproducibility and provenance

It is an often repeated tenet that results of scientific research must be reproducible. This objective is, however, challenging, especially in high-throughput research, due to the large number of simulations involved and the complex sequence of logical steps needed in the study. To ensure reproducibility we use AiiDA³⁰ as a materials' informatics infrastructure to implement the ADES model of automation, data, environment, and sharing, as discussed in Ref. 30. All input information for each calculation is stored in the AiiDA repository before calculations are launched and actual code inputs are created by AiiDA using only data already stored in the repository. However, even the ability to replicate single calculations is not sufficient, since the majority of results are obtained via long sequences of simulations. It is thus essential to persist the full provenance of each data item. This means, for instance, that for any 2D material identified in this work one can track from which 3D parent structure it originated (including its source database), how the structure was processed to obtain its coordinates from the Wyckoff positions, how the low-dimensional units were identified, and which parameters were used to compute the DFT results.

B. CIF files reformatting

The CIF files provided in crystallographic databases sometimes contain syntax errors or unnecessary information that needs to be corrected and/or removed before parsing them. To do so, we use `cod-tools`³², in particular the `cif_filter` and `cif_select` scripts, in order to:

- fix common CIF syntax errors,
- parse and reformat the summary chemical formula (from the tag `_chemical_formula_sum`),
- set explicit 90 degrees cell angles if they are not given (following the standard CIF specifications),
- remove empty non-loop tags,
- remove CIF data blocks without coordinates,
- convert non-standard CIF tag name capitalization into the capitalization specified by the CIF dictionary, for example `_atom_site_cartn_x` would be replaced by `_atom_site_Cartn_x`.

We also remove the tags `_publ_author_name` and `_citation_journal_abbrev`, that often contain problematic characters for, e.g., the `pymatgen` CIF parser (this information is still stored in the AiiDA database and therefore fully searchable).

As already mentioned in the main text, in this step we consider only structures coming from experimental measurements, while the source databases are partially populated by purely theoretical structures. This is done using the flags set on the database entries by their curators. We also implemented some heuristics to detect clearly wrong CIF files. For example, we discard structures where the chemical formula provided in the file is inconsistent with the elements in the unit cell. Regardless of all these efforts, it is possible that some incomplete or incorrect structures are still not filtered out from the original databases.

C. Crystal structure refinement

The crystal structures parsed from CIF files are often subject to round-off errors in the atomic positions and/or cell parameters that artificially lower the number of symmetries. We use the `spglib` software³⁴ to refine each structure and recover the maximum number of symmetries, using the algorithm described in Ref. 51. Interatomic distances and cell parameters are modified by at most $5 \cdot 10^{-3}$ Å with respect to the initially parsed structure. At the same time (and with the same software), a standardised crystallographic primitive cell is extracted⁵².

D. Removal of duplicates and prototyping

For the duplicate filtering procedure of both 3D and 2D structures, as well as for the prototyping of 2D structures, we have used extensively the “structure matcher” of `pymatgen`³³, which, thanks to the algorithm described in Ref. 35, compares crystal structures. The goal is to 1) reduce the two structures to be compared to their primitive cells, 2) rescale the volumes (if 3D), or the in-plane areas (if 2D), 3) find, when it exists, an affine map between the two cells, within certain tolerances on the cell lengths and angles, and 4) compute the maximum distance between atomic sites when the two lattices are mapped onto a common average lattice. If this maximum is lower than a certain fraction of the average free length per atom, then the two structures are classified as similar.

When comparing 3D structures, the tolerances on cell lengths, cell angles, and distances between paired atomic sites were chosen to be 20%, 5° and 30% of the average free length per atom, defined as the cubic root of the volume per atom. For 2D structures, due the artificial vacuum added to the cell in the out-of-plane direction the relative tolerances needed to be set tighter, and we chose 10%, 1° and 10%, respectively.

To filter out duplicates of a set of structures, all compounds with same composition (i.e., the same species in the same relative proportion) are compared among them using the structure-matcher algorithm, forming groups of

matching structures. One unique structure is then chosen in each group as a representative for further calculations.

The same tool is used to prototype 2D structures, but with a number of modifications: 1) two structures must have the same space-group to be considered as members of the same prototypical class (we used spglib with a precision parameter of 0.5 Å to get the space-group, see above), 2) the comparison is made irrespective of the specific species on each atomic site (e.g., MoS₂ and WTe₂ are both considered as AB₂), 3) when the two primitive cells do not contain the same number of sites, one also attempts to generate a supercell of the smaller lattice before the mapping, and 4) the tolerances on respectively the cell lengths, cell angles and maximum distance between sites are set to 10%, 5° and 20% respectively. Again all structures of the same kind of composition (e.g., AB₂, A₂B₃, etc.) are compared in pairs, to classify them into distinct prototypical classes.

E. DFT calculations

We use the Quantum-ESPRESSO distribution⁵³ with the SSSP efficiency pseudopotentials' library⁵⁴ (version 0.7). This library of extensively tested pseudopotentials from various sources^{55–60} provides to date the best overall agreement with respect to all-electron calculations^{61,62}. Wavefunction and charge-density cutoffs are chosen according to convergence tests with respect to cohesive energies, stresses and phonon frequencies performed for

each individual element⁵⁴.

Two different van-der-Waals functionals are employed, namely the vdW-DF2-C09^{38–40} and the revised VV10^{41–43}, in addition to the PBE⁴⁴ and revPBE⁴⁵ functionals. k -point sampling of the Brillouin zone is set using a Γ -centred Monkhorst-Pack grid, with an even number of k points in each direction of the reciprocal lattice such that the spacing between two consecutive k points along each direction is as close as possible to 0.2 Å⁻¹. A Marzari-Vanderbilt cold smearing⁶³ of 0.02 Ry is used. All calculations are done without considering spin polarization and spin-orbit coupling. When isolating 2D substructures, a vacuum space of 20 Å is set along the orthogonal direction to remove any fictitious interaction between periodic images of the 2D layers.

IV. ACKNOWLEDGEMENTS

This work was supported by the MARVEL National Centre of Competence in Research of the Swiss National Science Foundation. Simulation time was provided by the Swiss National Supercomputing Centre (CSCS) under project IDs mr0 and ch3, amounting to 3.7 million core hours to complete this study. The authors would also like to thank Davide Campi for his help in evaluating the stability of unaries, as well as Francesco Ambrosio, Antimo Marrazzo and Thibault Sohier for many useful discussions.

-
- ¹ Radisavljevic, B., Radenovic, A., Brivio, J., Giacometti, V. & Kis, A. Single-layer MoS₂ transistors. *Nature Nanotechnology* **6**, 147–150 (2011).
- ² Liu, H. *et al.* Phosphorene: An unexplored 2D semiconductor with a high hole mobility. *ACS Nano* **8**, 4033–4041 (2014).
- ³ Wang, Q. H., Kalantar-Zadeh, K., Kis, A., Coleman, J. N. & Strano, M. S. Electronics and optoelectronics of two-dimensional transition metal dichalcogenides. *Nat. Nanotech.* **7**, 699–712 (2012).
- ⁴ Chhowalla, M., Jena, D. & Zhang, H. Two-dimensional semiconductors for transistors. *Nature Reviews Materials* **1**, 16052 (2016).
- ⁵ Butler, S. Z. *et al.* Progress, challenges, and opportunities in two-dimensional materials beyond graphene. *ACS nano* **7**, 2898–2926 (2013).
- ⁶ Geim, A. & Grigorieva, I. Van der Waals heterostructures. *Nature* **499**, 419–425 (2013).
- ⁷ Villars, P., Onodera, N. & Iwata, S. The Linus Pauling file (LPF) and its application to materials design. *Journal of Alloys and Compounds* **279**, 1–7 (1998).
- ⁸ Inorganic Crystal Structure Database (ICSD). <http://www.fiz-karlsruhe.com/icsd.html>.
- ⁹ Gražulis, S. *et al.* Crystallography open database (COD): an open-access collection of crystal structures and platform for world-wide collaboration. *Nucleic Acids Research* **40**, D420–D427 (2012).
- ¹⁰ Lebègue, S., Björkman, T., Klintonberg, M., Nieminen, R. M. & Eriksson, O. Two-dimensional materials from data filtering and ab initio calculations. *Physical Review X* **3**, 031002 (2013).
- ¹¹ Miró, P., Audiffred, M. & Heine, T. An atlas of two-dimensional materials. *Chemical Society Reviews* **43**, 6537–6554 (2014).
- ¹² Rasmussen, F. A. & Thygesen, K. S. Computational 2D Materials Database: Electronic structure of transition metal dichalcogenides and oxides. *The Journal of Physical Chemistry C* (2015).
- ¹³ Gould, T., Lebègue, S., Björkman, T. & Dobson, J. 2D structures beyond graphene: The brave new world of layered materials and how computers can help discover them. In Iacopi, F., Boeckl, J. J. & Jagadish, C. (eds.) *2D Materials*, vol. 95 of *Semiconductors and Semimetals*, chap. 1, 1 – 33 (Elsevier, 2016).
- ¹⁴ Franceschetti, A. & Zunger, A. The inverse band-structure problem of finding an atomic configuration with given electronic properties. *Nature* **402**, 60–63 (1999).
- ¹⁵ Johannesson, G. H. *et al.* Combined electronic structure and evolutionary search approach to materials design. *Physical Review Letters* **88**, 255506 (2002).
- ¹⁶ Curtarolo, S., Morgan, D., Persson, K., Rodgers, J. & Ceder, G. Predicting crystal structures with data min-

- ing of quantum calculations. *Physical Review Letters* **91**, 135503 (2003).
- 17 Curtarolo, S. *et al.* The high-throughput highway to computational materials design. *Nature Materials* **12**, 191–201 (2013).
 - 18 Jain, A., Shin, Y. & Persson, K. A. Computational predictions of energy materials using density functional theory. *Nature Reviews Materials* **1**, 15004 (2016).
 - 19 Mueller, T., Hautier, G., Jain, A. & Ceder, G. Evaluation of tavorite-structured cathode materials for lithium-ion batteries using high-throughput computing. *Chemistry of Materials* **23**, 3854–3862 (2011).
 - 20 Saal, J., Kirklin, S., Aykol, M., Meredig, B. & Wolverton, C. Materials design and discovery with high-throughput density functional theory: The Open Quantum Materials Database (OQMD). *JOM* **65**, 1501–1509 (2013).
 - 21 Ozolins, V., Majzoub, E. H. & Wolverton, C. First-principles prediction of thermodynamically reversible hydrogen storage reactions in the Li-Mg-Ca-B-H system. *Journal of the American Chemical Society* **131**, 230–237 (2009).
 - 22 Greeley, J., Jaramillo, T. F., Bonde, J., Chorkendorff, I. & Norskov, J. K. Computational high-throughput screening of electrocatalytic materials for hydrogen evolution. *Nature Mater.* **5**, 909–913 (2006).
 - 23 Greeley, J. *et al.* Alloys of platinum and early transition metals as oxygen reduction electrocatalysts. *Nature Chem.* **1**, 552–556 (2009).
 - 24 Yu, L. & Zunger, A. Identification of potential photovoltaic absorbers based on first-principles spectroscopic screening of materials. *Physical Review Letters* **108**, 068701 (2012).
 - 25 Castelli, I. E. *et al.* New light-harvesting materials using accurate and efficient bandgap calculations. *Advanced Energy Materials* **5**, 1400915–n/a (2015).
 - 26 Zhuang, H. L. & Hennig, R. G. Computational search for single-layer transition-metal dichalcogenide photocatalysts. *The Journal of Physical Chemistry C* **117**, 20440–20445 (2013).
 - 27 Novoselov, K. S. *et al.* Electric field effect in atomically thin carbon films. *Science* **306**, 666–669 (2004).
 - 28 Coleman, J. N. *et al.* Two-dimensional nanosheets produced by liquid exfoliation of layered materials. *Science* **331**, 568–571 (2011).
 - 29 Bonaccorso, F. *et al.* Production and processing of graphene and 2D crystals. *Materials Today* **15**, 564 – 589 (2012).
 - 30 Pizzi, G., Cepellotti, A., Sabatini, R., Marzari, N. & Kozinsky, B. AiiDA: automated interactive infrastructure and database for computational science. *Computational Materials Science* **111**, 218 – 230 (2016).
 - 31 Hall, S. & McMahon, B. (eds.). *International Tables for Crystallography*, vol. G (Springer, 2005).
 - 32 Merkys, A. *et al.* COD::CIF::Parser: an error-correcting CIF parser for the Perl language. *Journal of Applied Crystallography* **49** (2016).
 - 33 Ong, S. P. *et al.* Python Materials Genomics (pymatgen): A robust, open-source python library for materials analysis. *Computational Materials Science* **68**, 314–319 (2013).
 - 34 Togo, A. <http://spglib.sourceforge.net>.
 - 35 Hundt, R., Schön, J. C. & Jansen, M. CMPZ—an algorithm for the efficient comparison of periodic structures. *Journal of applied crystallography* **39**, 6–16 (2006).
 - 36 O’Keeffe, M. & Hyde, B. *Crystal Structures I. Patterns and Symmetry* (Mineralogical Society of America, 1996).
 - 37 Alvarez, S. A cartography of the van der Waals territories. *Dalton Transactions* **42**, 8617–8636 (2013).
 - 38 Lee, K., Murray, É. D., Kong, L., Lundqvist, B. I. & Langreth, D. C. Higher-accuracy van der Waals density functional. *Physical Review B* **82**, 081101 (2010).
 - 39 Cooper, V. R. Van der Waals density functional: An appropriate exchange functional. *Physical Review B* **81**, 161104 (2010).
 - 40 Hamada, I. & Otani, M. Comparative van der Waals density-functional study of graphene on metal surfaces. *Physical Review B* **82**, 153412 (2010).
 - 41 Vydrov, O. A. & Van Voorhis, T. Nonlocal van der Waals density functional made simple. *Physical Review Letters* **103**, 063004 (2009).
 - 42 Vydrov, O. A. & Van Voorhis, T. Nonlocal van der Waals density functional: The simpler the better. *The Journal of chemical physics* **133**, 244103 (2010).
 - 43 Sabatini, R., Gorni, T. & de Gironcoli, S. Nonlocal van der Waals density functional made simple and efficient. *Physical Review B* **87**, 041108 (2013).
 - 44 Perdew, J. P., Burke, K. & Ernzerhof, M. Generalized gradient approximation made simple. *Physical Review Letters* **77**, 3865–3868 (1996).
 - 45 Zhang, Y. & Yang, W. Comment on “generalized gradient approximation made simple”. *Physical Review Letters* **80**, 890–890 (1998).
 - 46 Björkman, T., Gulans, A., Krasheninnikov, A. V. & Nieminen, R. M. van der Waals bonding in layered compounds from advanced density-functional first-principles calculations. *Physical Review Letters* **108**, 235502 (2012).
 - 47 Arguilla, M. Q. *et al.* NaSn₂As₂: An Exfoliatable Layered van der Waals Zintl Phase. *ACS Nano* **10**, 9500–9508 (2016).
 - 48 Dion, M., Rydberg, H., Schröder, E., Langreth, D. C. & Lundqvist, B. I. van der Waals density functional for general geometries. *Physical Review Letters* **92**, 246401 (2004).
 - 49 Nicolosi, V., Chhowalla, M., Kanatzidis, M. G., Strano, M. S. & Coleman, J. N. Liquid exfoliation of layered materials. *Science* **340** (2013).
 - 50 Cordero, B. *et al.* Covalent radii revisited. *Dalton Transactions* 2832–2838 (2008).
 - 51 Grosse-Kunstleve, R. W. & Adams, P. D. Algorithms for deriving crystallographic space-group information. II. treatment of special positions. *Acta Cryst. A* (2002).
 - 52 Hinuma, Y., Togo, A., Hayashi, H. & Tanaka, I. Choice of basis vectors for conventional unit cells revisited. *arXiv:1506.01455* (2015).
 - 53 Giannozzi, P. *et al.* QUANTUM ESPRESSO: a modular and open-source software project for quantum simulations of materials. *Journal of Physics: Condensed Matter* **21**, 395502 (2009).
 - 54 Castelli, I. E. *et al.* Standard solid state pseudopotentials (SSSP). URL <http://www.materialscloud.ch/sssp/>.
 - 55 Garrity, K. F., Bennett, J. W., Rabe, K. M. & Vanderbilt, D. Pseudopotentials for high-throughput DFT calculations. *Computational Materials Science* **81**, 446 – 452 (2014).
 - 56 Kucukbenli, E. *et al.* Projector augmented-wave and all-electron calculations across the periodic table: a comparison of structural and energetic properties. *arXiv:1404.3015* (2014).

- ⁵⁷ Dal Corso, A. Pseudopotentials periodic table: From H to Pu. *Computational Materials Science* **95**, 337–350 (2014).
- ⁵⁸ Schlipf, M. & Gygi, F. Optimization algorithm for the generation of ONCV pseudopotentials. *Computer Physics Communications* **196**, 36 – 44 (2015).
- ⁵⁹ Willand, A. *et al.* Norm-conserving pseudopotentials with chemical accuracy compared to all-electron calculations. *The Journal of Chemical Physics* **138** (2013).
- ⁶⁰ Topsakal, M. & Wentzcovitch, R. Accurate projected augmented wave (PAW) datasets for rare-earth elements (RE = La-Lu). *Computational Materials Science* **95**, 263 – 270 (2014).
- ⁶¹ Lejaeghere, K. *et al.* Reproducibility in density functional theory calculations of solids. *Science* **351** (2016).
- ⁶² Lejaeghere, K., Van Speybroeck, V., Van Oost, G. & Cottenier, S. Error estimates for solid-state density-functional theory predictions: An overview by means of the ground-state elemental crystals. *Critical Reviews in Solid State and Materials Sciences* **39**, 1–24 (2014).
- ⁶³ Marzari, N., Vanderbilt, D., De Vita, A. & Payne, M. C. Thermal contraction and disordering of the al(110) surface. *Physical Review Letters* **82**, 3296 (1999).